# THERMAL ANALYSIS OF A PUMPED LIMITER

## THE EXPERIENCE OF THE USE OF THE MSC/NASTRAN SOLUTION 89

BY

SOLOMON DINKEVICH AND AHMED SHAABAN
EBASCO Services Incorporated
New York, New York, 10048

To increase the efficiency of the surface pumping panels installed in the TFTR Vacuum Vessel, it was proposed to add a perpendicular scraper blade (Neutralizer Plate) as a reflector. The blade would extend in the space above the surface pumping panels towards the plasma.

The Neutralizer plate, being close to the plasma will be subjected by particle collection to a very high heat flux of impulsive and repetitive nature. To define a probable configuration of the blade, the thermal and structural analysis was conducted using the MSC/NASTRAN computer code (solutions 89 and 24, respectively)

Several important peculiarities of Solution 89 were found during the test. They are:

1. Varying levels of required accuracy in computation of view factors for different quadrilateral finite elements.
2. Large amounts of the CPU time for the calculation of the radiation matrix.
3. The necessity to eliminate the radiation matrix recomputation and therefore to avoid new cold runs in the case of temperature-dependent materials when the thermal conduction matrix has to be recalculated several times.
4. Sensitiveness of the solution to high heat flux gradients on finite elements that provokes a numerical instability of the process.

This paper discusses those complexities and how they were overcome. It also contains the solution to the above problem.

## I. INTRODUCTION

The Tokamak Fusion Test Reactor (TFTR) is expected to achieve reactor like operating conditions and explore some reactor relevent technologies. Its primary components are Vacuum Vessel (toroidal vacuum chamber), Toroidal and Poloidal Field Coils, Neutral Beam and so on (Fig. 1).

The ability of the TFTR to attain the highest plasma temperature and largest fusion power gain depends upon minimizing plasma contamination and controlling the densities of reacting deuterium and tritium. To achieve this, the TFTR Surface Pumping System (SPS) composed of 36 pumping panels will be mounted throughout the vacuum vessel.

The cross-section of the vacuum vessel, two surface pumping panels, and three special plasma configurations (scenarios) are shown in Figure 2.

To increase the efficiency of the SPS the pumped limiter concept was created. The pumped limiter as a particle reflector is expected to remove a significant portion of the atoms injected during a discharge. The pumped limiter as a system of scraper blades (also called Neutralizer Plates) extends in the space above the surface pumping panels towards the plasma. Since the poloidal particle velocities along the magnetic field lines are hundred times larger than their toroidal velocities, it is sufficient to install scraper blades only on two of the 36 surface pumping panels. They are shown in Fig. 2.

The pumped limiter must withstand high thermal and mechanical loads associated with plasma disruption, runaway electrons, and unattenuated neutral beam strikes. To find a reliable blade configuration, the thermal and structural analysis was performed using the MSC/NASTRAN computer code (solutions 89 and 24, respectively).

The paper discusses the modelling of the problem. It presents some solution 89 difficulties which were found and overcome during the job execution. Some recommendation to avoid such difficulties are also given.

## II. THE MODELING OF THE PROBLEM

The initial configuration of the scraper blade is given in Fig. 3a. The material of the blade is Inconel X-750 [1]. This is a temperature-dependent material, its conductivity versus temperature is presented in Fig. 4. The blade thickness is h = .159cm.

The scraper blade receives the energy from the plasma by particle collection. The heat flux which is induced on the blade is determined by the following equation [2]:

$$Q_r = \frac{P}{2\pi\lambda a} e^{-(r-a)/\lambda} , \qquad (1)$$

where

$Q_r$ is the heat flux at the point of the blade($w/cm^2$),

P is the plasma power (Mega Watt),

$\lambda$ is the particle scrape-off distance (cm),

a is the plasma minor radius (cm),

r is the distance from the plasma center to the point of the blade (cm).

Three plasma scenarios had to be considered. They are described by their major and minor radii (see Table 1). Sets of given parameters P and $\lambda$ were analyzed, the most significant of them are P = 5 Megawatts and $\lambda$ =2 cm.

The heat flux was induced on the blade by the 1.5 sec. pulses. Recycle time was equal to 300 seconds (Fig. 5).

The total energy applied to the blade is distributed along its surface by conduction. A significant part of this energy is lost through radiation.

To simulate this event in the model, the scraper blade was confined in a special absorbing box, with its top open (Fig. 6). Besides its geometry, this artificial box is characterized by the vacuum emissivity parameter of $\varepsilon_3$=.99. Such high value of emissivity is chosen to eliminate any energy reflection from the box to the blade. The surface pumping panel was placed on the top of the box with a small real gap between them. Other emissivity values are $\varepsilon_1$ = .9 for the surface pumping panel (its material is stainless steel), and $\varepsilon_2$ = .2 for the scraper blade (INC X-750).

The boundary temperatures are: $T_1$ = 350°C on the surface pumping panel, and $T_2$ = 150°C on the box sides.

## III. THE SCRAPER BLADE CONFIGURATION

Eq. (1) is now used to calculate heat flux distributions on the blade for three given plasma scenarios. Contour lines of the constant heat flux are plotted in Fig. 7a, b, and c for all cases. High crowding of contour lines at the edge region is explained by heat flux exponential term dependency in radial distance r (see eq (1) ).

It immediately follows from Fig. 7, that the second and third plasma scenarios produce very high heat fluxes which will destroy the blade. Hence, the blade initial configuration must be changed.

The previous experience with Inconel X-750 testifies that temperature increments for a pulse should not exceed ~450°C. Based upon this criterion we can find the highest acceptable magnitude of the heat flux at any point on the blade. The following equation of the energy storage in a solid may be used for this purpose:

$$Q = ch\frac{\Delta T}{\Delta t} \qquad (2)$$

Here $Q$ is the heat flux $(\frac{W}{cm^2})$,

$c$ is the thermal capacity $(\frac{W - sec}{cm^3 \times °C})$,

$h$ is the thickness of the blade (cm),

$\Delta T$ is the temperature increment (°C),

$\Delta t$ is the time increment (sec).

For the given data, c = 3.56, h = .158, T=450., t = 1.5, the acceptable heat flux magnitude is equal to Q=170 W/cm$^2$. Thus we can conclude that the initial blade (Fig. 3a) is suitable for the first plasma scenario only. Therefore, the blade was cut along the contour line, Q=170 w/cm$^2$, for the second and third plasma scenarios (Fig. 7b and c) which enabled us to find an allowable scraper blade configuration for the further analysis. The reduced blade is shown in Fig. 3b.

## IV. THE FINITE ELEMENT MODEL

The model of the abosorbing box is characterized by 18 grid points, and by 10 boundary surface elements (Table 2). The box grid point boundary temperatures are introduced by large conductive couplings to the "ground" (QHBDY2 and CELAS cards).

The scraper blade is described by the 2-D models, the first model, BM1, is shown in Fig. 3c. This curvilinear model was used in the structural analysis only. However, for thermal analysis it was replaced by thermally equivalent trapesoidal like model, BM2, (Fig. 8a) in order to reduce computer time for the radiation matrix calculation. Each element of this model has the same area as the corresponding elements of BM1. Characteristics of those models are presented in Table 2.

Note that the expansion slots of small width were described by double grid points with the same coordinates (Fig. 3a and Fig. 8). For example, grid points 1104 and 1105 have the same coordinates.

After several tentative runs, it was concluded that a number of time steps for the 300 seconds pulse cycle may be minimized by using four non-equal intervals with a constant time increment for each (Table 3).

It was found, during the solution of the problem that 11 pulses were needed to achieve the temperature equilibrium at each grid point. Thus, a total number of time steps was 6790.

To end the BM2 description, note that (a) boundary surface elements (HBDY cards) overlay both surfaces of the conduction elements, and (b) head flux is specified at the vertices of the elements (by QBDY2 cards).

## V. PECULIARITIES OF SOLUTION 89

The Thermal Analysis of the scraper blade described above was performed by Solution 89, "transient heat transfer with radiation". This solution is based upon the following thermal equilibrium equation [3]:

$$B\dot{u} + Ku = P + R\left(4\left[(u_a + T_a)^3\right]u - (u + T_a)^4\right) \qquad (3)$$

Here B is the thermal capacitance matrix,

K is the thermal conduction matrix,

R is the radiation matrix,

u is the vector of temperature at grid points,

$T_a$ is the vector of additional temperature to convert u to an absolute temperature scale,

P is the applied load.

The difficulties which arise in Solution 89 for our problem may be divided into two parts:

(a) difficulties produced by the calculation and/or recalculation of matrices R, K and B,

(b) convergence and stability of the numerical solution of eq (3).

## V-1 THE CALCULATION OF THE RADIATION MATRIX

In our case, MSC/NASTRAN's calculation of the matrix R was the most costly module. It took from 40 to 95.5 percent of the total CPU time.

To build the matrix R we need to compute view factors. According to [3], a total view factor supplied for an element should not exceed 1.001, since a fatal message will abort the run in most of the versions.*) To get such high accuracy for view factors, we increased a number of subelements (parameters HB and HG on VIEW cards) and introduced a small value for the parameter $R_{max}$ through the PARAM, RMAX card. Unfortunately we could not get the required view factor accuracy for a reasonable CPU time of 35-45 minutes on the CRAY1 computer. The smallest view factor value which was obtained for this CPU time was 1.0025, and the fatal messages aborted the run.

Fortunately, it was found that all fatal messages were associated with trapesoidal elements. Neither triangular nor rectangular elements generated this fatal message even when their view factors achieved the value of 1.100. Therefore, we created a new rectangular like blade model, BM3,(see Fig. 8b). This model uses rectangular and triangular elements only. Its characteristics are given in Table 2. Although a total number of elements has increased by 25%, the CPU time for view factors was reduced to 2.3 minutes, that is, to 40% of the total CPU time.

It is necessary to note, that the model BM3 is not thermally equivalent to the previous one, yet it is more conservative. Areas of the cold elements for BM3 (the upper strip of elements) are 3% less than areas of the BM2 corresponding elements, while the areas of the BM3 hot elements (the edge strip of elements) are larger by 4 to 8% when compared to the same BM2 elements. Obviously such level of conservativeness is quite reasonable for the engineering purposes.

## V-2 THE RECALCULATION OF THE THERMAL CONDUCTION MATRIX K

Solution 89 creates the matrix K only once for the initial temperature conditions. It does not account for the automatic recalculation of K when temperature-dependent materials are used in the analysis, and as described in [3], "it was judged to be excessive." According to the recommendation of MSC, Solution 89 in such cases has to be augmented by the RFALTER (the RFOD75 card in the executive Control Deck).

However, we could not utilize this because of the excessive computer time needed in one run. We used an iterative process with several runs, considering the final temperatures from the previous one as the initial temperatures for the next run. The thermal conductivity for the Inc X-750 is a quasi constant function of temperature (see Fig.4). It's slope is above $1.43 \times 10^{-4}$ watt/cm/K°. Thus only two iterations were necessary.

It is very important to note, that the second run for each plasma scenario was restarted so as to eliminate the recomputation of the radiation matrix R. In accordance with the recommendation of MSC, we altered out statements 288 to 298, and introduced the SEMG card in the Case Control Deck.

*) MSC/NASTRAN version 62A was used in this analysis.

THE EXECUTIVE CONTROL DECK

```
.............
SOL 89
ALTER 288, 298
CEND
```

THE CASE CONTROL DECK

```
.............
SET 71 = 0
SEMG = 71
.............
```

The typical graphs of the temperature functions are plotted in Fig. 9a,b,c, and d for the cold, warm, and hot grid points 105, 705, 1105 and 1305 which lie on the radial line of the angle 78°.

## V-3 THE RECALCULATION OF THE THERMAL CAPACITANCE MATRIX B

Besides the initial blade thickness $h_1$ = .159cm, we also considered the double thickness, $h_2$ = .318cm. for the special plasma scenario #1A with the .75 sec. pulses. Since the scraper blade was simulated by the 2-D models, any change of it's thickness cannot influence the radiation matrix R. To bypass it's recalculation, we tried to utilize restart as was described above. However, the results did not change from those of the initial thickness, indicating that the matrix B was not recalculated during this restart, although the conductivity element volumes were doubled.

MSC recommended to add the SEMR card in the Case Control Deck.

The new restart with

THE EXECUTIVE CONTROL DECK

```
.............
SOL 89
ALTER 288,298
CEND
```

THE CASE CONTROL DECK

```
.............
SET 71 = 0
SEMG = 71
SEMR = 71
.............
```

computed new temperatures versus time at every grid point. They are shown in Fig. 10b and 11b for grid point 705 and 913, respectively. The original temperature curves corresponding to the initial blade thickness, $h_1$ = .159cm, are given in Figures 10a and 11a for the same grid points. As seen from these figures, the temperature increment for each pulse is reduced by a factor of two, as it has to be in accordance with eq (2):

$$\frac{\Delta T_2}{\Delta T_1} = \frac{h_1}{h_2} = \frac{1}{2}$$

Thus, the capacitance matrix B was correctly recalculated.

However, as it follows from Fig. 10b and 11b, in the case of a double blade thickness, the temperature equilibrium is not achieved after 11 pulses. This leads to conclusion on our part that the results which were obtained by the restart run may be wrong. A new cold run with the recomputed matrix R resulted in temperature functions which are very compatable with the original functions corresponding to the initial blade thickness $h_1$ = .159cm. They are shown in Fig. 10c and 11c for the same grid points 705 and 913, and as seen, the temperature equilibrium was achieved after 11 pulses at each grid point. Thus it is concluded that the above recalculation of the matrix B by a restart run produced the numerical instability of the process.

Note that the valley temperatures practically did not change, in comparison with the corresponding temperatures of the initial blade thickness, while their peak values reduced in accordance with eq (2).

## V-4 CONVERGENCE AND STABILITY OF THE NUMERICAL SOLUTION

The BM3 model gave correct results for the first and third plasma scenarios only. In the case of the second plasma scenario incorrect temperatures versus time values were obtained at several grid points. Three of those curves are plotted in Fig. 12a, b, and c for grid points 121, 715 , and 717, respectively. As can be seen from the figures, the addition of the heat flux to the blade by new pulses reduces temperature and even causes it to be negative. This points to the numerical instability; although the process is convergent, but it converges to the wrong values.

According to [3], the method used in Solution 89 is very close to the Newmark $\beta$ method. It's convergence, stability, and accuracy depend basically on the parameter $\beta$ , $0 < \beta < 1$, and the time step, $\Delta t$. The default value of $\beta = .55$ was maintained for all calculations. The assumption that time steps changes would help to overcome instability did not materialize, and the same temperatures versus time values were obtained.

In search of the instability reasons, the distribution of the heat flux of the three plasma scenarios were constructed as shown in Fig. 13a,b,c. In the figure it is seen that the total heat flux was clearly not the problem because that value is comparable in the two first cases, and even much less than that of the third case. Second, the highest heat flux intensity of 128 w/cm$^2$ in the 2nd case is less than the 162 w/cm$^2$ of the 3rd case, thus indicating that heat flux intensity could not be the reason. However, the principal difference between both the first and third scenarios on one hand, and the second on the other, is demonstrated by the configuration of the contour lines for the constant heat flux. In the first and third cases they are almost parallel to sides of the finite elements, while in the second case they follow the diagonals of the elements with much higher gradients across the elements. Hence, we have to conclude that Solution 89 is sensitive to the element heat flux gradients.

Thus it became clear how to overcome this problem. One more model of the blade, BM4, was created especially for the second plasma scenario (Fig. 8a). All right hand side elements of the previous BM3 model were divided into three or four elements to reduce the magnitudes of the element heat flux

gradients. The characteristics of this model are given in Table 2. The model BM4 gave very reasonable temperatures versus time values for all blade grid points. They are plotted in Fig. 14a, b, and c for the same grid points 121, 715, and 717 for which we had wrong results in the model BM3.

Finally, we point out that the view factor computation for this model took 55.61 minutes of the CRAY1 CPU time, i.e 95.5% of the total.

## VI RESULTS OF THE SCRAPER BLADE ANALYSIS

The peak values of the final temperature distributions are plotted in Fig. 15a, b, and c for all three plasma scenarios. The structural analysis that followed showed acceptable thermal stresses and very small displacements. Thus, it was found that expansion slots were not necessary.

## VII. CONCLUSION

The MSC/NASTRAN solution 89 demonstrated high capability, efficiency, and accuracy in the thermal analysis of the scraper blade. However, the following suggestions may be made for the future version of MSC/NASTRAN.

1. The algorithm for view factor computation has to be improved so that
   (a) it significantly reduces computer time, and
   (b) it requires the same, or almost the same, accuracy for the total view factor value for different plane elements.

Small negative diagonal elements of the radiation matrix R have no physical meaning and have to be automatically zeroed.

It is not necessary to print the correpsonding warning message 4536 because the total value of view factors are already printed, or at least allow the user to prevent it's printing.

2. Solution 89 has to be able to selectively update the K and/or B matrices after the user selected intervals of time steps or load steps, based on his particular problem. In our case, for example, it can be done after each two of three pulses.

3. It is necessary to document the influence of the element heat flux gradients for convergence and stability of the numerical process, and to provide the users with more determined recommendation on how to create a correct model.

## VIII. ACKNOWLEDGEMENT

The authors wish to express their graditude to J.A. Joseph of the MacNeal-Schwendler Co and P. Rogoff and J. Bialek of the Princeton Plasma Physics Laboratory for their discussions and help to solve the problem.

## REFERENCES

1. Huntington Alloys Handbook. Huntington Alloys Inc. 1970

2. J. L. Cecchi et. al. "Reduction of Recycling by Pumping at the PDX Limiter. Plasma Physics Laboratory of Princeton University, 1983.

3. NASTRAN Thermal Analysis Vol. 1 and 2, National Aerosnautics and Space Administration, Washington, D.C. 1977

TABLE 1 THREE PLASMA SCENARIOS

| PLASMA SCENARIO | THE MAJOR RADIUS R CM | THE MINOR RADIUS a CM |
|---|---|---|
| #1 | 265 | 75 |
| #2 | 305 | 55 |
| #3 | 258 | 82 |
| VACUUM VESSEL | 265 | 110 |

TABLE 2 CHARACTERISTICS OF FINITE ELEMENT MODELS OF THE ABSORBING BOX AND THE BLADE

| PARAMETERS | ABSORBING BOX | BLADE (2-D MODELS) | | |
|---|---|---|---|---|
| | | BM1 & BM2 | BM3 | BM4 |
| A NUMBER OF GRID POINTS | 18 | 48 | 48 | 71 |
| A NUMBER OF CONDUCTION ELEMENTS | – | 29 | 36 | 63 |
| A NUMBER OF BOUNDARY SURFACE ELEMENTS | 10 | 58 | 72 | 126 |

TABLE 3 TIME STEPS AND TIME INCREMENTS PER PULSE'S CYCLE

| # | TIME INTERVAL SEC | NUMBER OF TIME STEPS | TIME INCREMENT SEC |
|---|---|---|---|
| 1 | 0 - 3 | 300 | .01 |
| 2 | 3 - 23 | 200 | .1 |
| 3 | 23 - 50 | 54 | .5 |
| 4 | 50 - 300 | 125 | 2. |

*A TOTAL NUMBER OF TIME STEPS N = 6790*

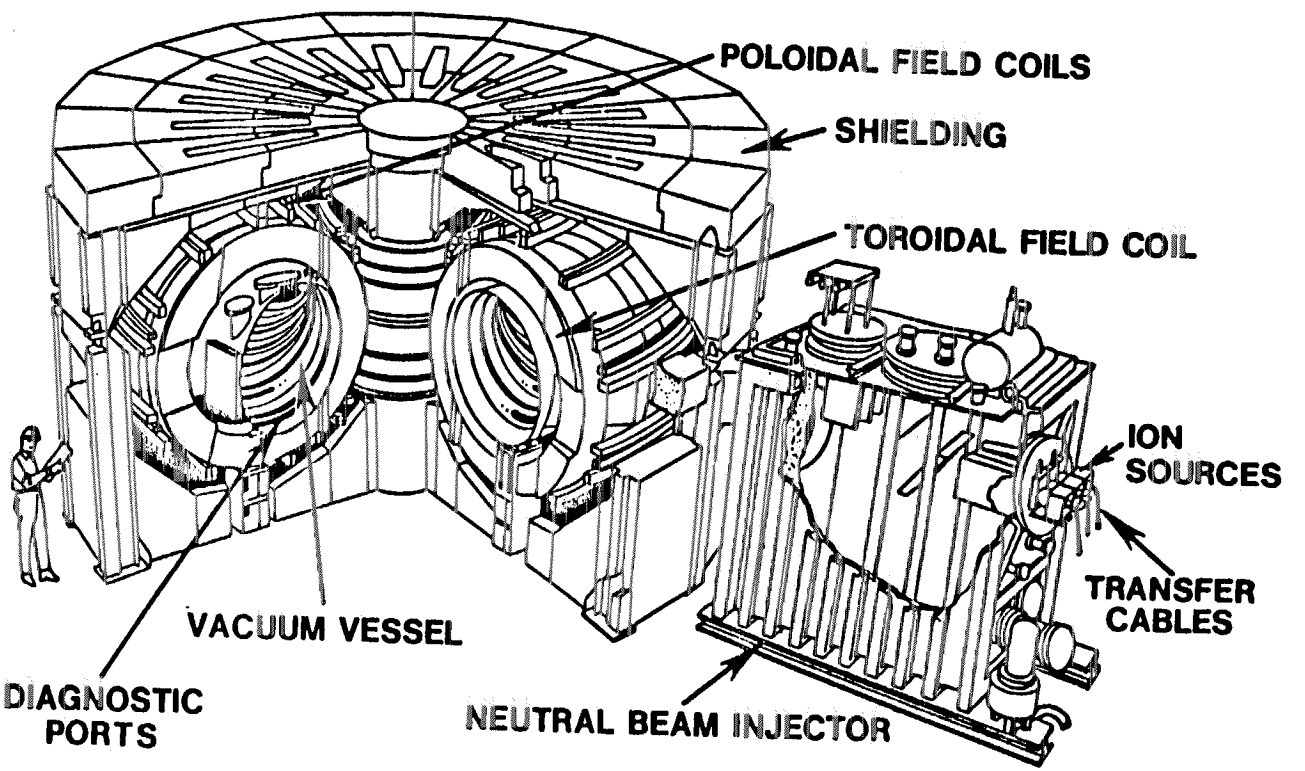


FIGURE 1 TOKAMAK FUSION TEST REACTOR (TFTR)

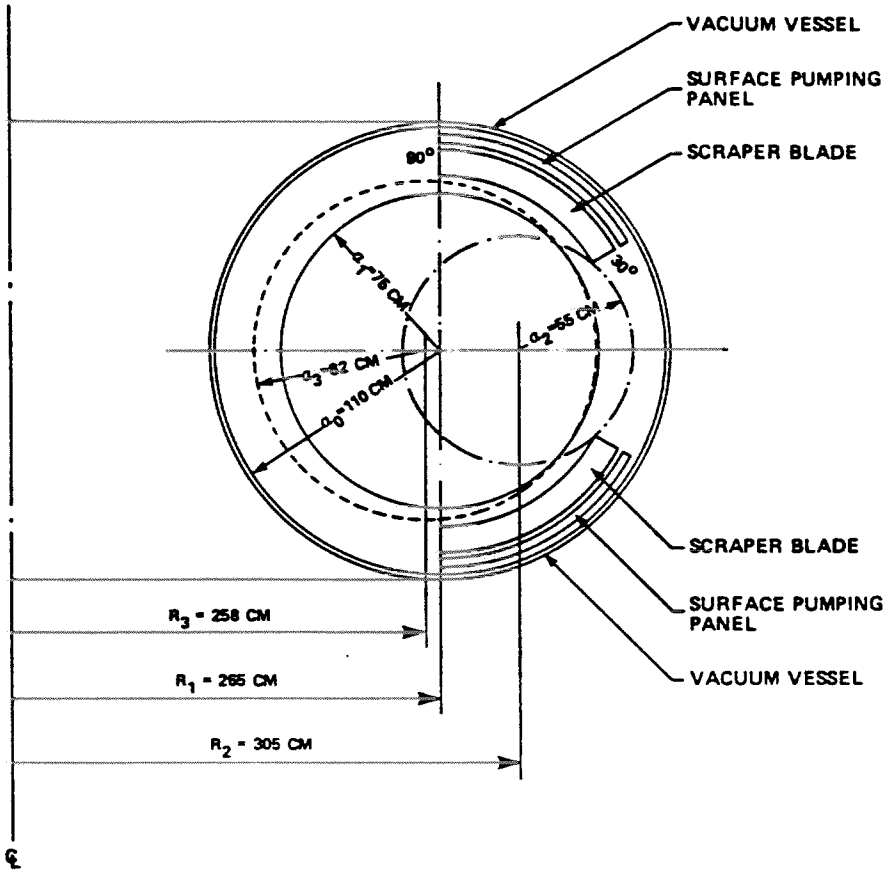


FIGURE 2 CROSS-SECTION OF A VACUUM VESSEL

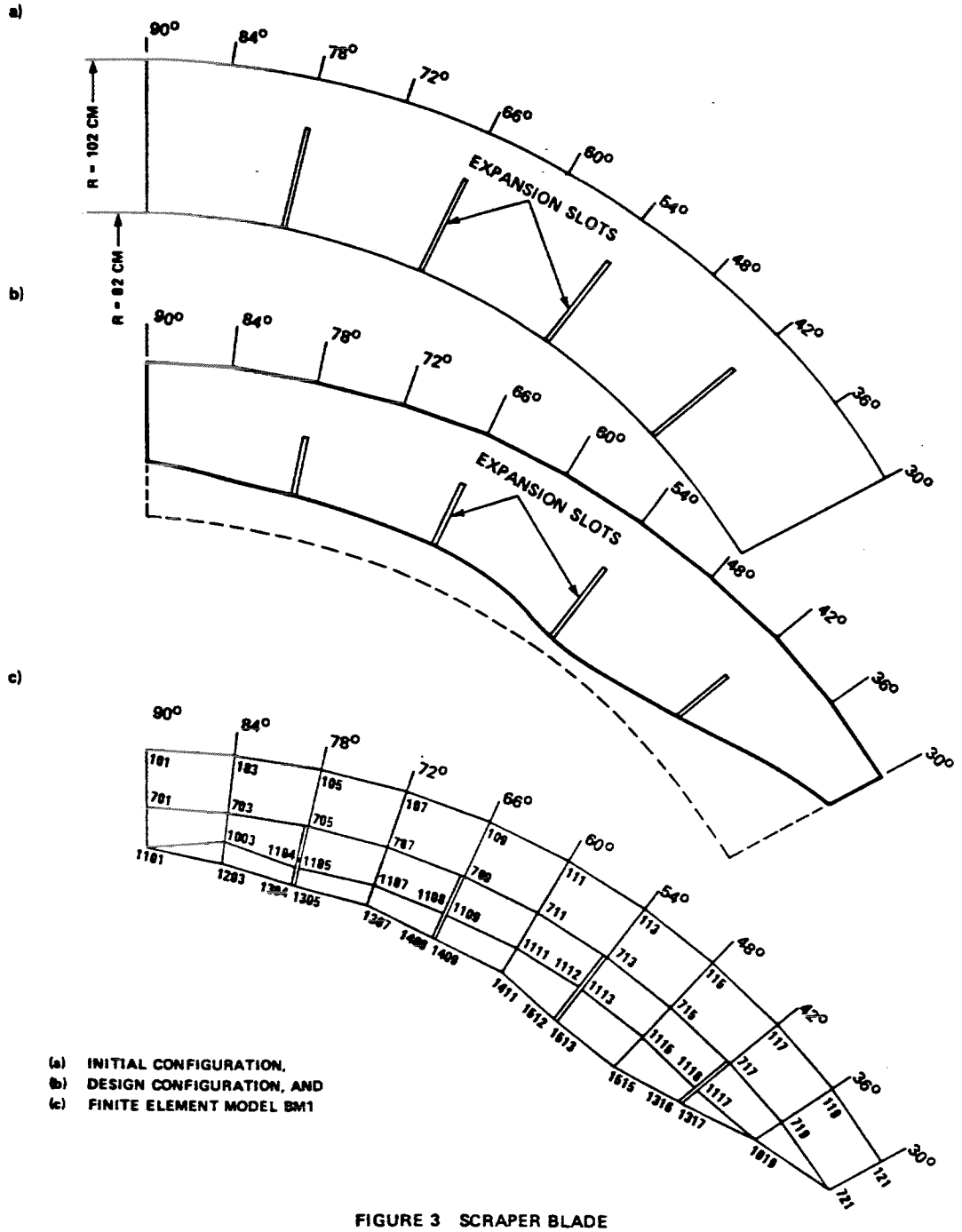


(a) INITIAL CONFIGURATION,
(b) DESIGN CONFIGURATION, AND
(c) FINITE ELEMENT MODEL BM1

FIGURE 3 SCRAPER BLADE

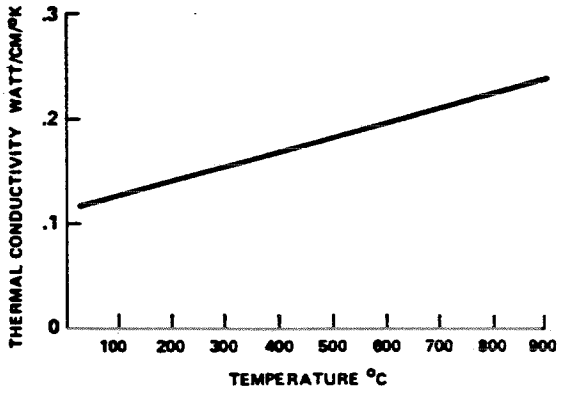


FIGURE 4 THERMAL CONDUCTIVITY vs TEMPERATURE FOR INC X-750

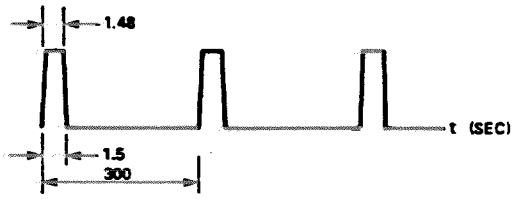


FIGURE 5 PULSE PROFILE AND PERIOD

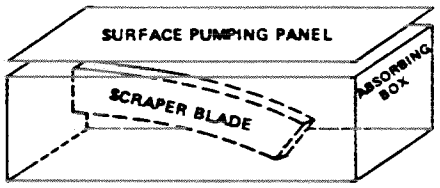


FIGURE 6 MODEL OF THE PROBLEM

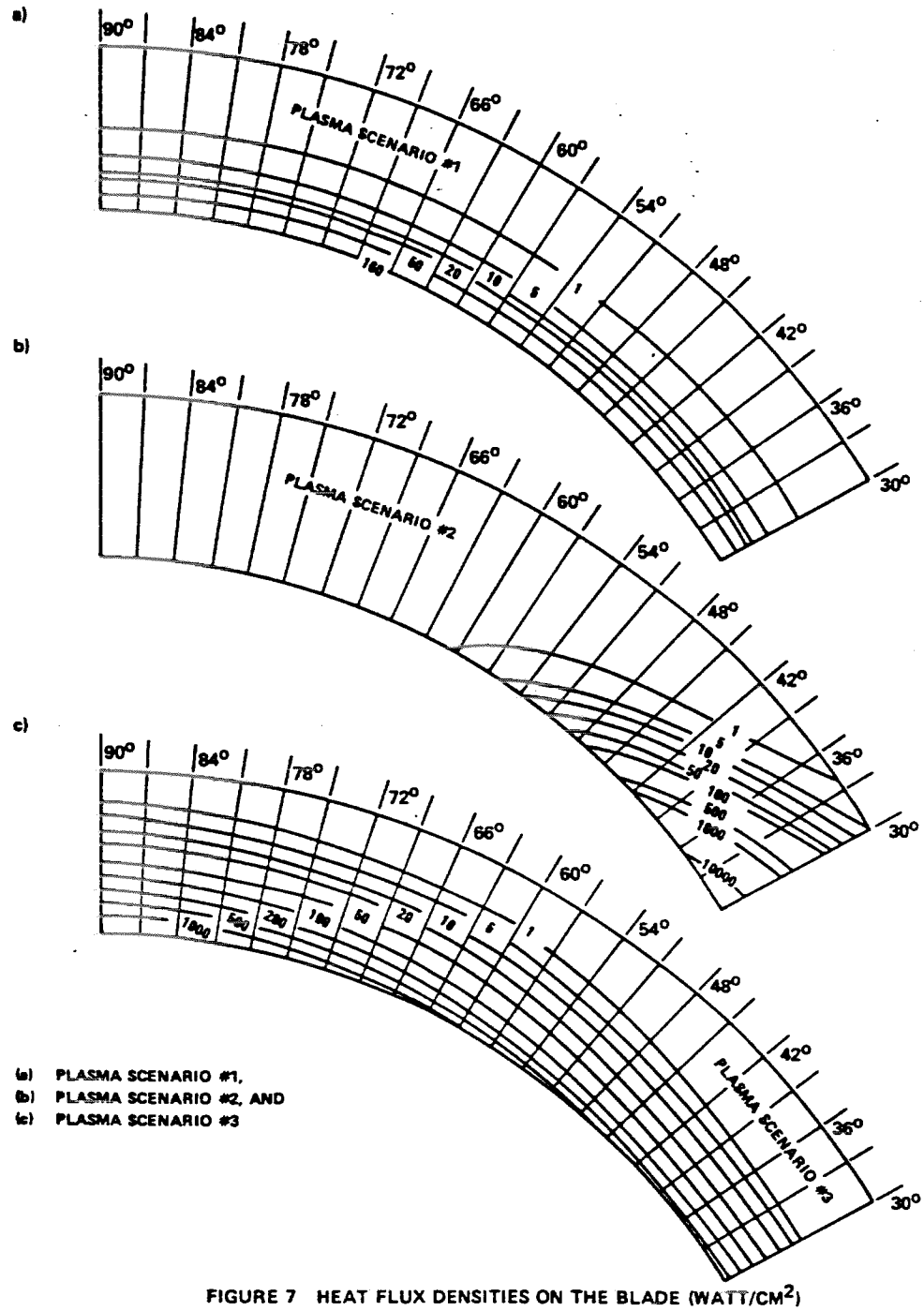


(a) PLASMA SCENARIO #1,
(b) PLASMA SCENARIO #2, AND
(c) PLASMA SCENARIO #3

FIGURE 7 HEAT FLUX DENSITIES ON THE BLADE (WATT/CM$^2$)

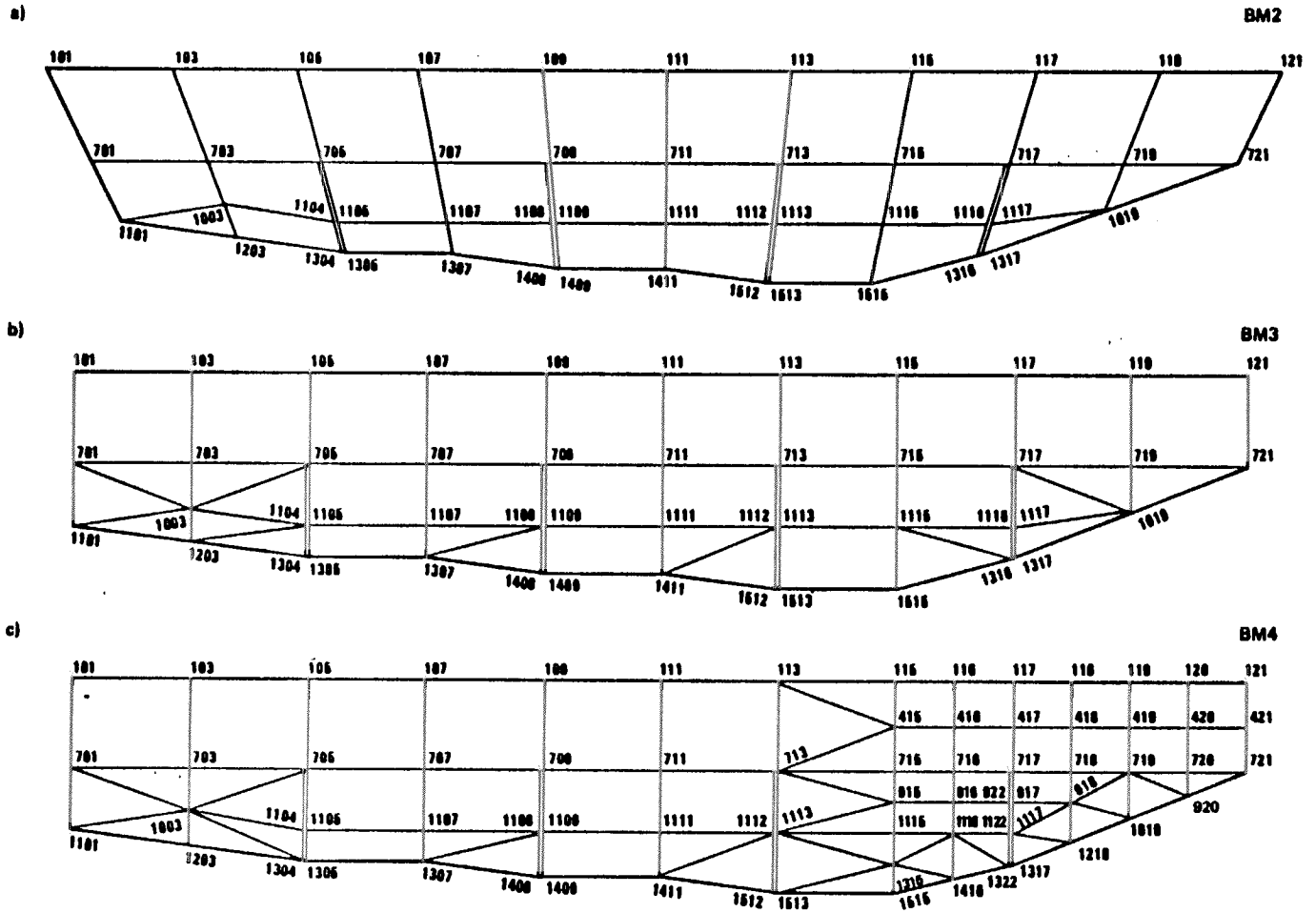


FIGURE 8 THREE FINITE ELEMENT MODELS OF THE BLADE

(a) MODEL BM2, (b) MODEL BM3, AND (c) MODEL BM4

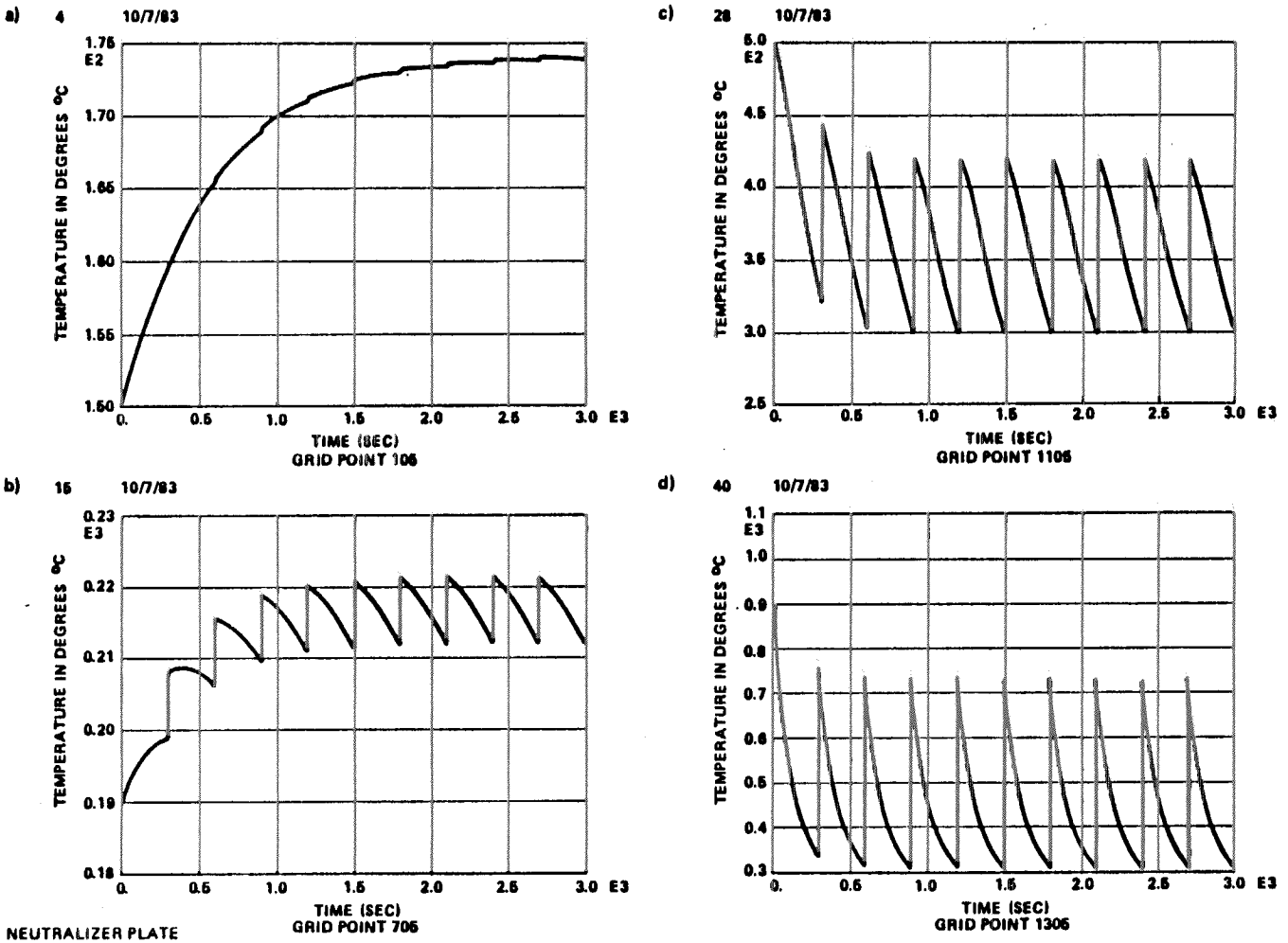


NEUTRALIZER PLATE
TRANSIENT HEAT FLUX WITH RADIATION
R0=268CM, A=82CM, PT=6MW, LAM=2CM,
PULSE=1.6 SEC

FIGURE 9 TEMPERATURE TIME-HISTORY
PLASMA SCENARIO #3, MODEL BM3

a)

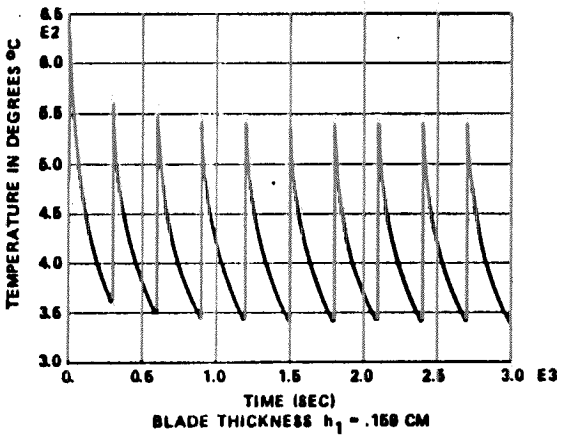


b)

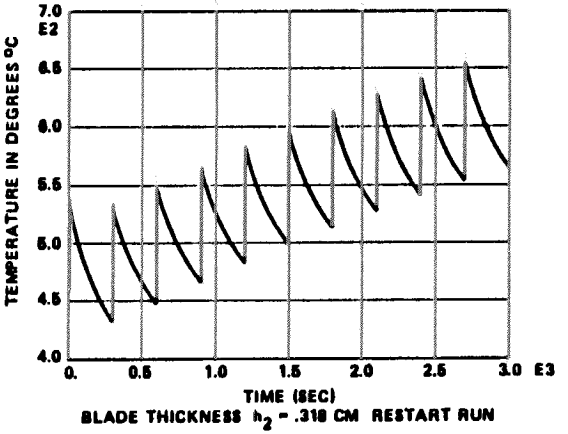


c)

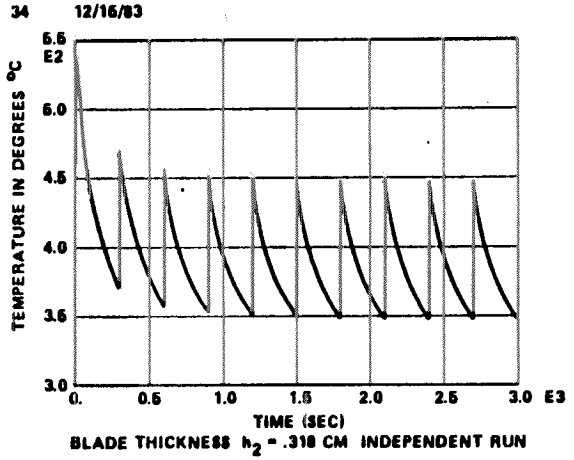


NEUTRALIZER PLATE
TRANSIENT HEAT FLUX WITH RADIATION
RO=248CM, A=87.2CM, PT=4.5MW, LAM=2CM, PULSE=.75 SEC

FIGURE 10 TEMPERATURE TIME HISTORY, GRID POINT 705
PLASMA SCENARIO # 1A, MODEL BM3

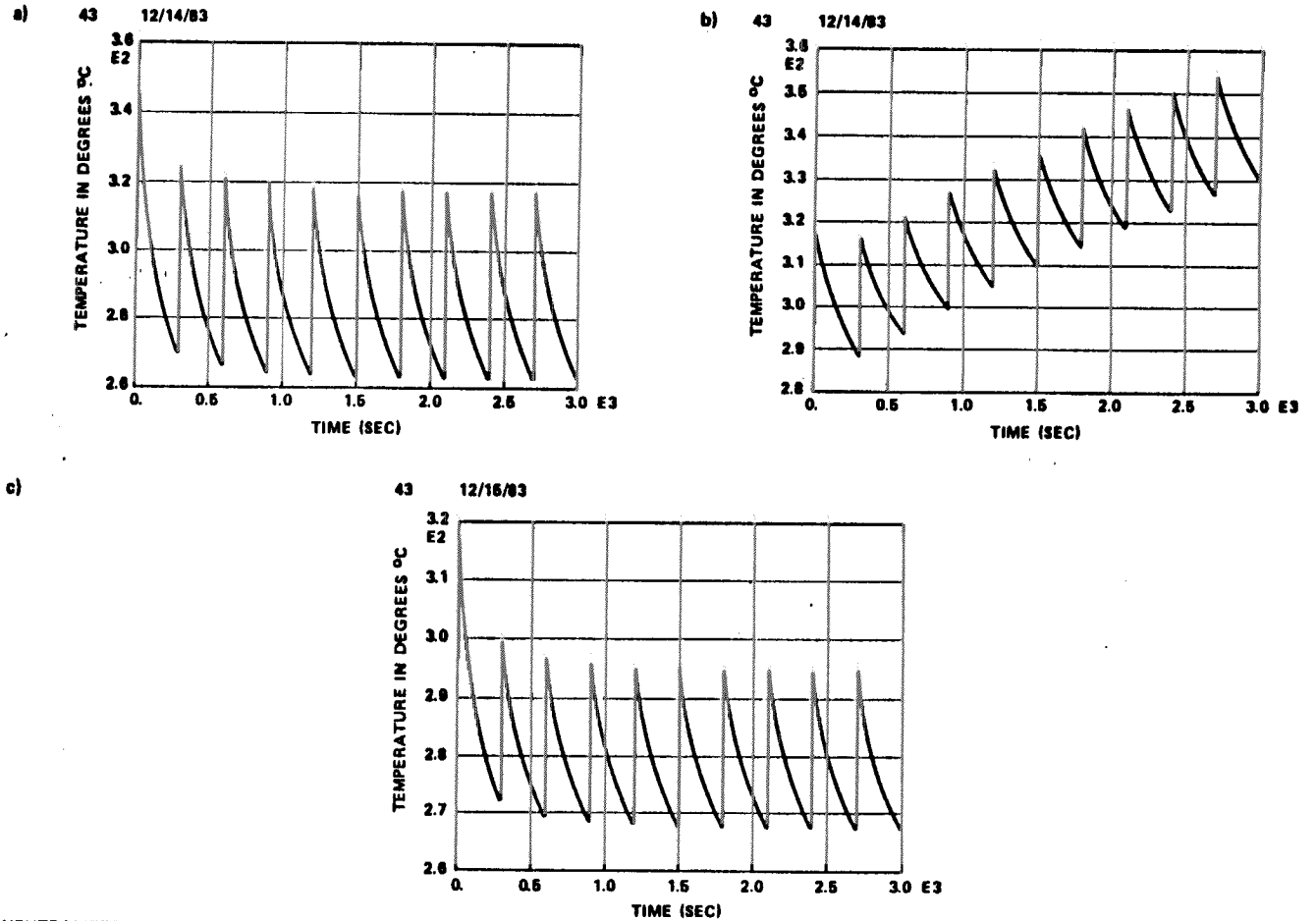


FIGURE 11 TEMPERATURE TIME-HISTORY, GRID POINT 913
PLASMA SCENARIO # 1A, MODEL BM3

a)

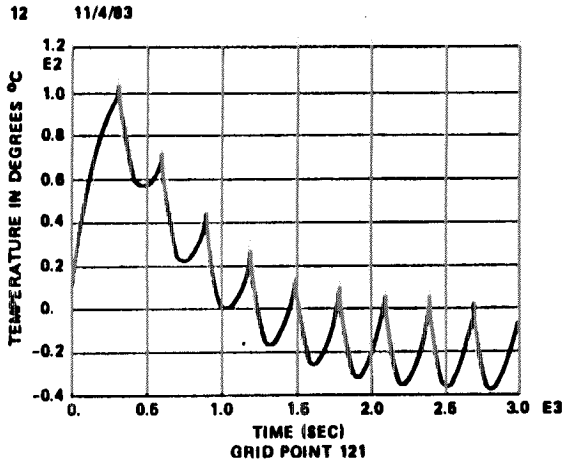


b)

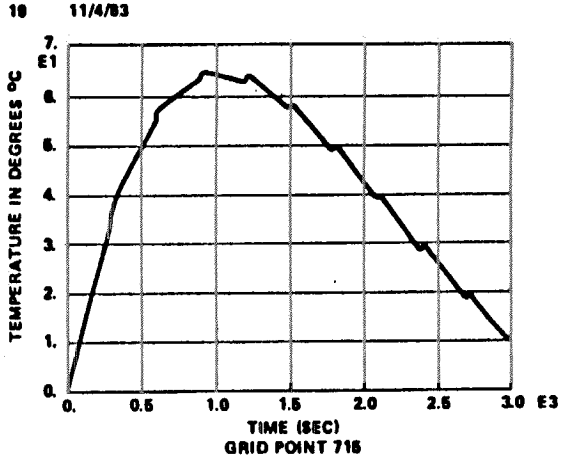


c)

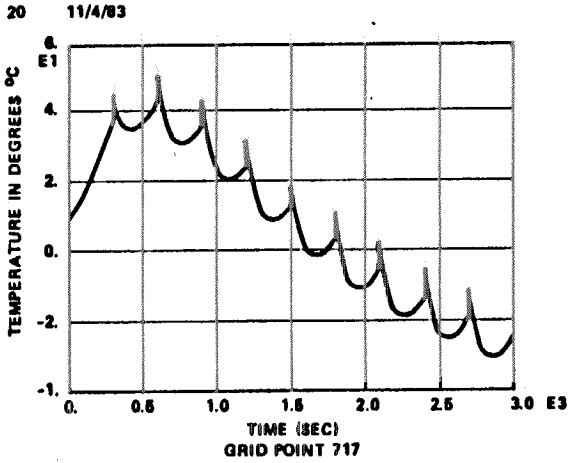


NEUTRALIZER PLATE
TRANSIENT HEAT FLUX WITH RADIATION
RO=305CM, A=56CM, PT=6MW, LAM=2CM, PULSE=1.5 SEC

**FIGURE 12 TEMPERATURE TIME-HISTORY PLASMA SCENARIO #2, MODEL BM3**

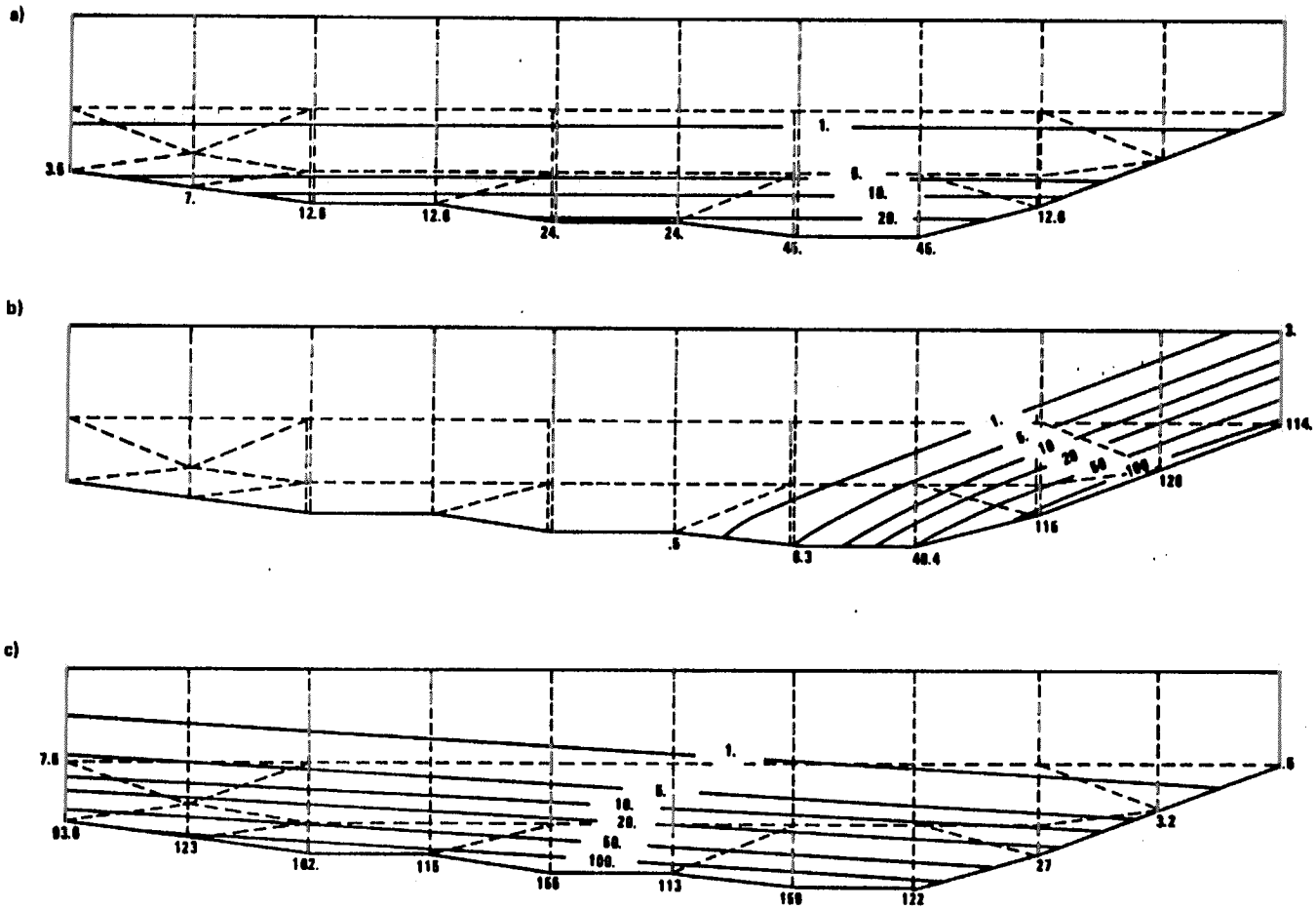


FIGURE 13 HEAT FLUX DENSITIES ON THE BLADE (WATT/CM$^2$)

(a) PLASMA SCENARIO #1,

(b) PLASMA SCENARIO #2, AND

(c) PLASMA SCENARIO #3

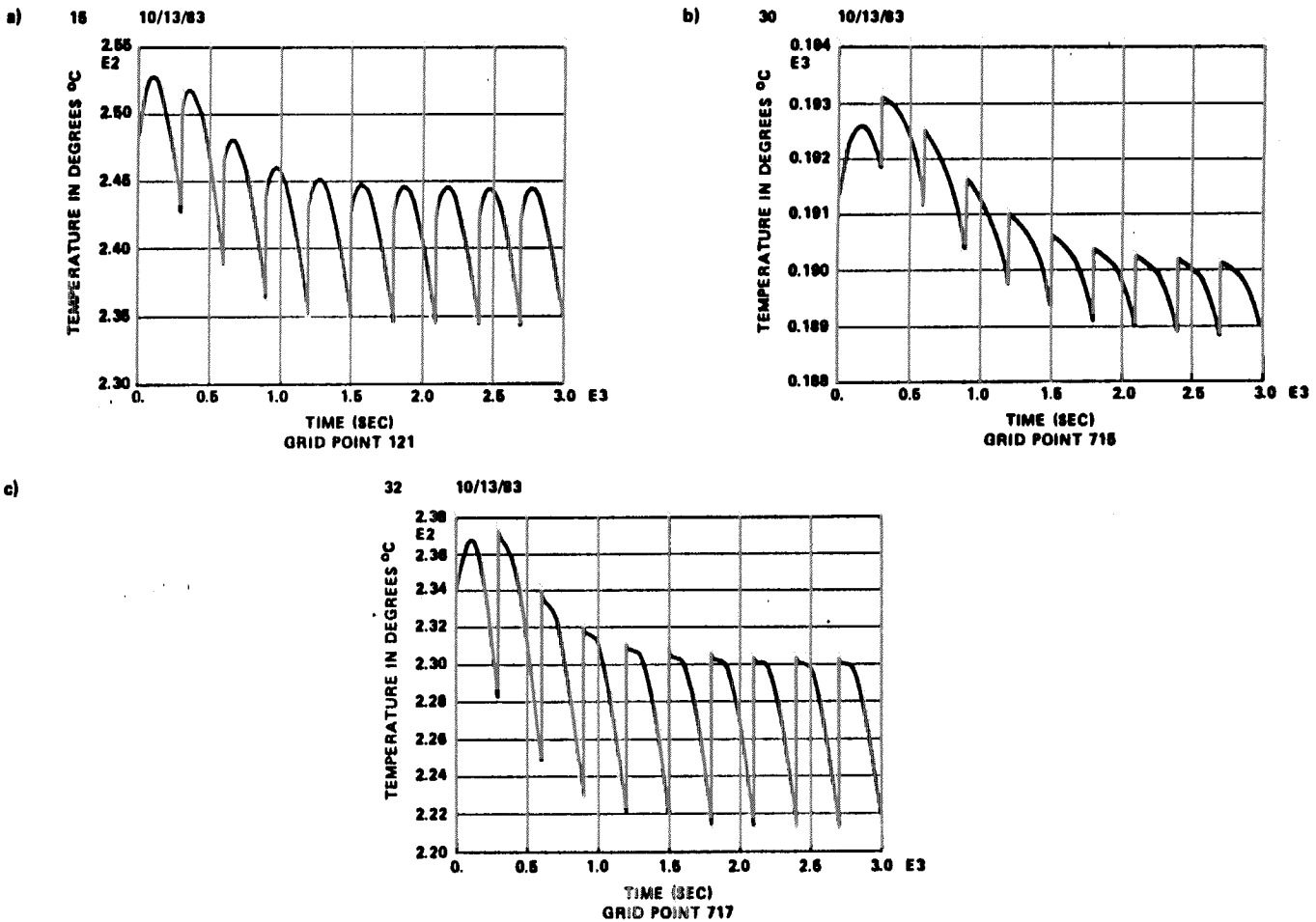


NEUTRALIZER PLATE
TRANSIENT HEAT FLUX WITH RADIATION
RO=305CM, A=55CM, PT=5MW, LAM=2CM, PULSE=1.5 SEC

FIGURE 14 TEMPERATURE TIME-HISTORY
PLASMA SCENARIO #2, MODEL BM3

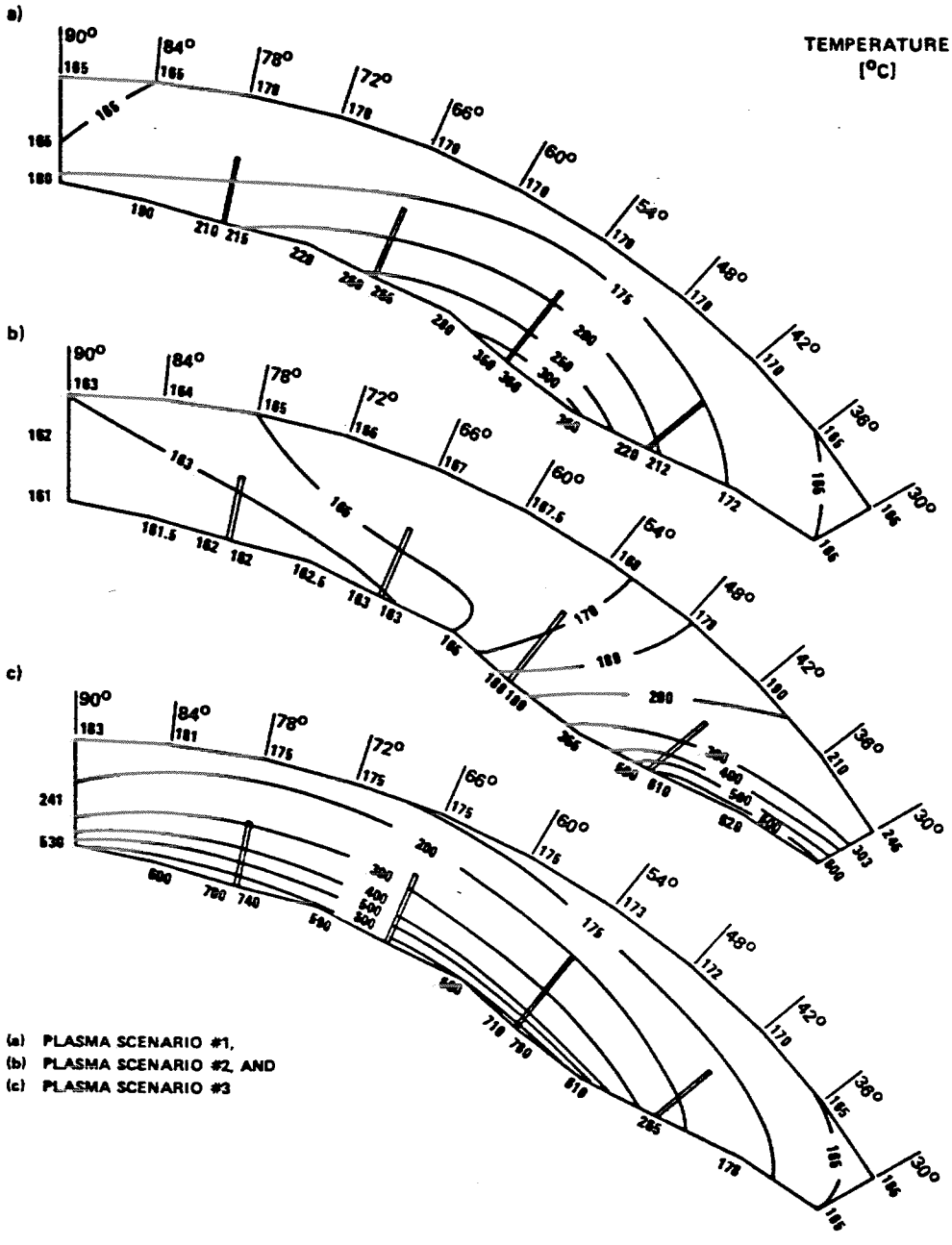


FIGURE 15 TEMPERATURE DISTRIBUTION ON THE BLADE, PEAK VALUES (°C)